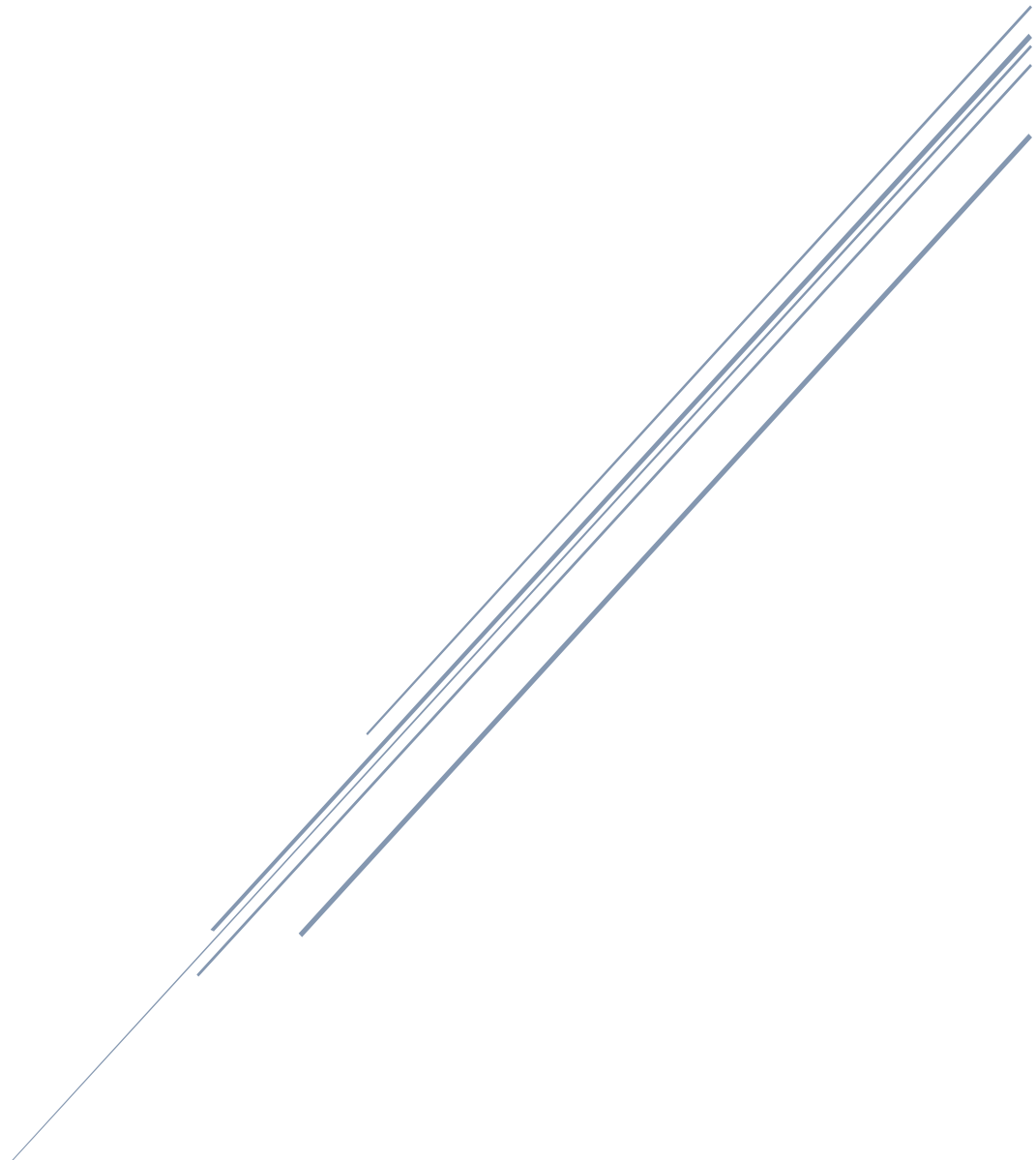


REPORT INTERNSHIP

CFD study on performance of a D.B.D. Plasma Actuated
airfoil in an ultra-low Reynolds number flow



UNIVERSITY OF TWENTE – ISAS/JAXA
INTERNSHIP

Table of contents

General introduction.....	2
Assignment introduction and approach	3
Determination of single zoned grid	5
Non-actuated airfoil performance and characteristics	7
Determination of double zoned grid.....	10
Actuated airfoil performance and characteristics	12
<i>Pre-stall results</i>	13
<i>Post-stall results</i>	17
Comparison non-actuated and actuated cases	22
Conclusion and recommendations.....	27
References	28

General introduction

This report contains the findings of my studies conducted at the Institute of Space and Astronautical Science, ISAS, in Japan as part of the mandatory internship during the last phase of the Mechanical Engineering program at the University of Twente. A more formal definition of such an internship is given by the ‘manual external training’ of the University of Twente and reads:

“The objective of an internship is to teach the student to function independently in a real life situation at graduate level in order to apply and increase their knowledge and competences. This knowledge and these competences are not only related to the student’s field of specialization, but also to people’s skills and to communication (both verbal and written) skills, possibly in a foreign language.”

It is in this light that I have been employed at ISAS from 2 December 2013 to 28 February 2014. As part of the Japan Aerospace Exploration Agency, JAXA, ISAS is an organization which focusses on the advancement of space science and planetary research. Founded in 1964 by the University of Tokyo, ISAS merged with the National Aerospace Laboratory of Japan, NAL, and the National Space Development Agency of Japan, NASDA, to form JAXA in 2003.

A vast amount of research is conducted at ISAS in various scientific fields, among which are a multitude of satellite programs and solar system explorers. The research presented in this report has been conducted at the Fujii laboratory which is part of the Department of Space Flight Systems at ISAS. The Fujii laboratory specializes in computational fluid dynamics and has contributed many publications to the scientific community. Currently, the Fujii laboratory is mainly divided into three groups. The first group conducts research into acoustic wave interference with payload during rocket launch. The second group works on the Marslander and the third group conducts research into flow separation control using dielectric barrier discharge plasma actuators. I have been working within the latter group.

My gratitude goes out to Professor K. Fujii who has accepted me as part of his research group. Also, Professor H.W.M. Hoeijmakers needs thanking for he has introduced me to ISAS/JAXA and whom without I would not have had this opportunity. Without the patient help and assistance of Ms. H. Tamura it would have been close to impossible for me to arrange all the details regarding my stay in Japan, also, many thanks for that. And last but definitely not least, a big thank you to all members of the Fujii laboratory who helped me with all practical issues which arose during the research.

Steven Rozeman

Assignment introduction and approach

Since the modern world of aviation got to accept the theory of flight after the first actual full flight on December 17th in 1903 by the Wright brothers, engineers have sought to improve flight performance on all possible levels thinkable. One of the ongoing fields of research in the improvement of flight performance is the field of flow separation control.

Separated flow occurs naturally in many situations caused by the boundary layer unable to overcome an adverse pressure gradient and thus becoming detached from the surface. Such separated flow comes with an array of undesirable effects such as increased (pressure) drag, a possible loss of lift and noise generation from shedded vortices. Controlling flow separation is therefore very important in achieving greater airfoil performance.

This study focusses on CFD simulation of flow separation control of an ultra-low Reynolds number flow over a NACA-0015 airfoil equipped with a dielectric barrier discharge (DBD) plasma actuator. To investigate effects of plasma actuation, actuator location and angles of attack are varied.

A DBD plasma actuator is an electronic device which uses a high electric potential between two electrodes, separated by a dielectric material, such that a flow of plasma is created between both electrodes. A schematic representation of this phenomena is shown in figure 1. This plasma induces a flow from the far field towards the surface which is deflected near the plasma region to be parallel to the dielectric surface. This induced airflow has a direct influence on the flow near the plasma actuator. As of yet, the plasma actuator is known to have three distinctive mechanisms which can influence separation behavior. Firstly, the induced flow can ‘help’ the boundary layer stay (more) attached to the airfoil surface by adding momentum to the boundary layer and thus to delay separation. Secondly, the induced flow can change the direction of the separated shear layer to be more aligned to the airfoil surface. Thirdly and lastly, the induced flow can promote the transition from laminar flow to turbulent flow.

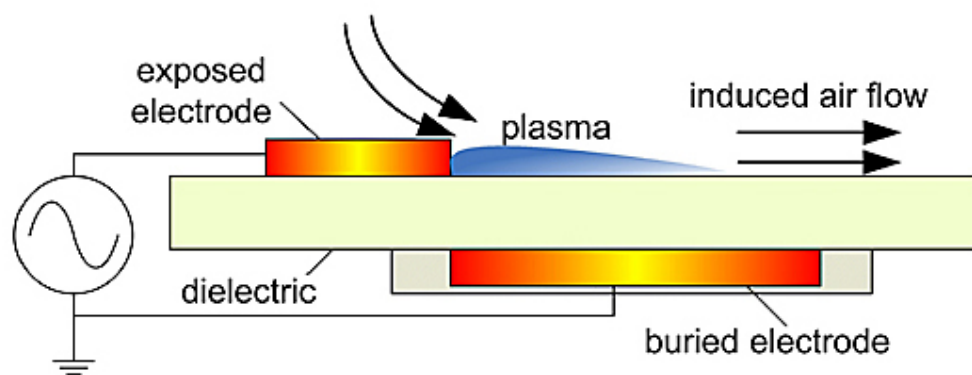


Figure 1: schematic of plasma actuator

One of the more elegant features of a DBD plasma actuator is that the representation in numerical solvers is relatively simple. The induced flow is simply added to the conservation equations by means of a body force. Since this study is about using an existing solver, there will be no further elaboration on the implementation of the plasma actuator in the CFD code.

The CFD code is an ISAS in-house code which incorporates the (slightly modified) Suzen & Huang plasma actuator model.

Now we return to the assignment and the approach. Because the topic of research can be massively diverse and time-consuming, certain restrictions and limitations have been imposed on the study. First of all, previous works conducted by members of the Fujii laboratory have been on NACA-0015 airfoils with flows of Reynolds numbers 63000, 260000 and 1600000. To complement this range of flows, an ultra-low Reynolds number case should be added to the existing portfolio. Also, since ultra-low Reynolds number flows might be approximated as being laminar, it is acceptable to conduct 2D simulations only. This saves considerable time compared to fully 3D simulations and since this project only takes three months, time is of the essence. From this reasoning, a flow of Reynolds number 1000 has been selected.

From a bird's eye view, the research is of the following form. To investigate effects of plasma actuation, all cases are compared with non-actuated, or reference, cases. These reference cases are simply the airfoil without plasma actuator with a flow of Reynolds number 1000 and varying angles of attack. Different plasma actuated cases are of varying actuator location and of varying actuator mode. Two actuator modes are employed, normal mode actuation and burst mode actuation. In normal mode, the potential over both electrodes is constant over time and the induced airflow is continuous. In burst mode, the potential over both electrodes is applied for only a specific period of the convective time (the time it takes for a flow element to travel one chord's length). Also, it should be noted that all work is purely numerical. No experimental validation or verification has been done, nor is there any available experimental data to compare with.

Determination of single zoned grid

All simulations are conducted on a grid surrounding the airfoil surface. The grid is a C-type structured mesh, having 425 lines in j-direction, 3 lines in k-direction and 91 lines in l-direction. This totals to 110625 grid points. Without going into detail of every parameter, a schematic representation on how the C-type grid is constructed, is given in figure 2. It shows which parameters can be chosen and how others depend on such choices. Creating the grid proved to be very time consuming. In figure 2 an overview of the complete grid is given and in figure 3 a more detailed view of the grid near the airfoil surface is shown.

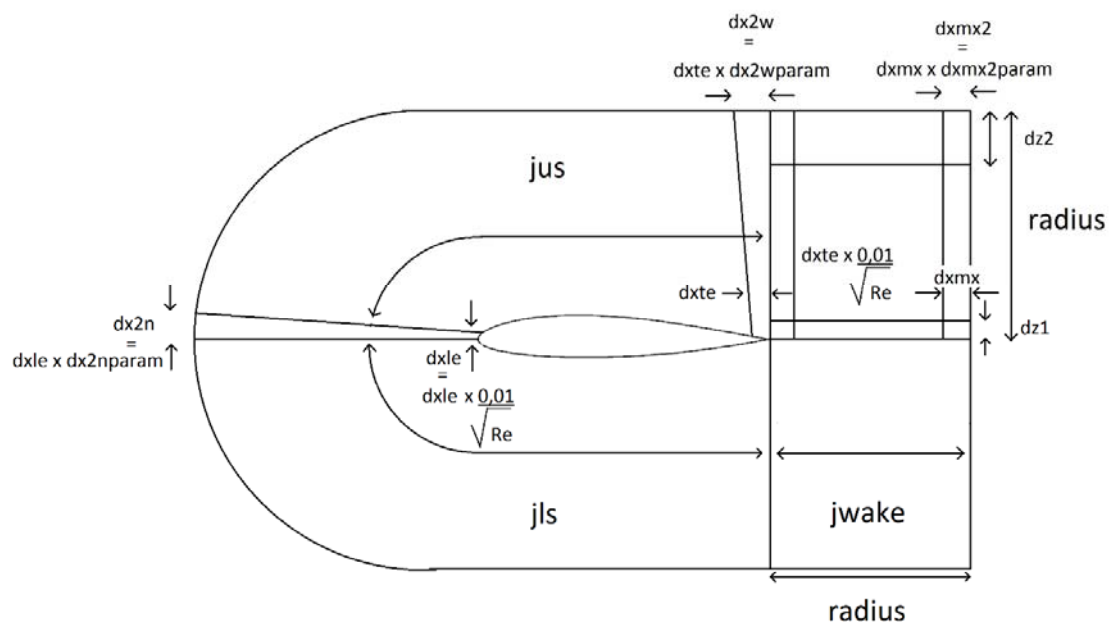


Figure 2: grid layout and parameters

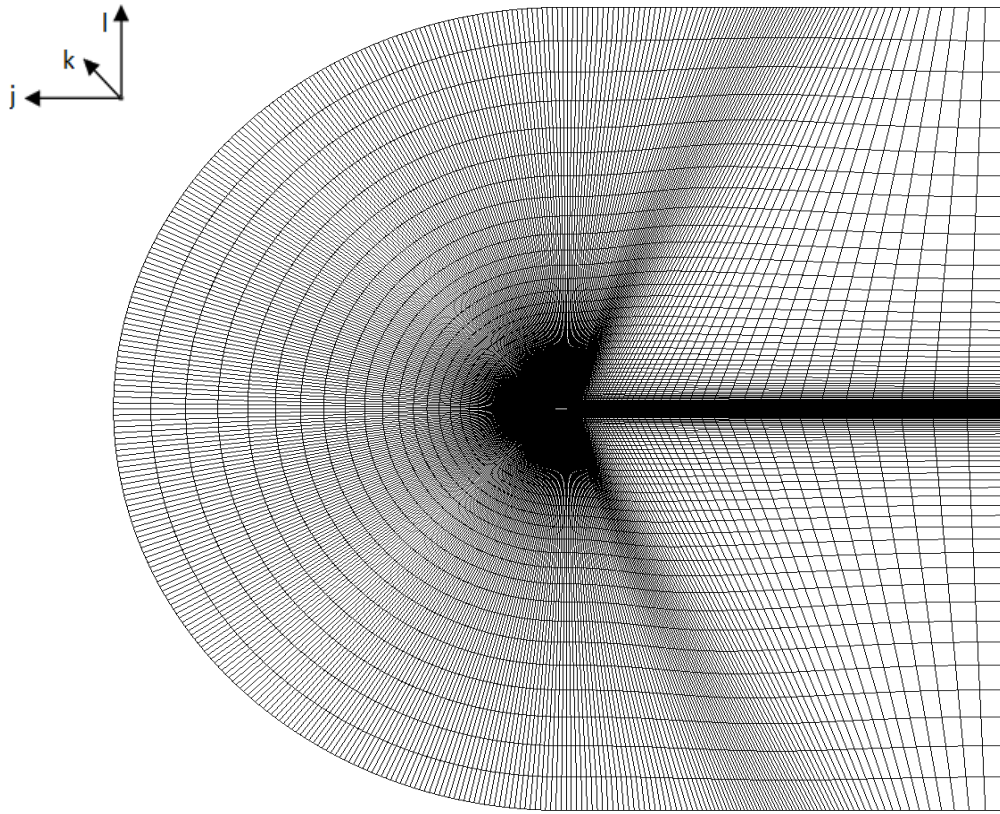


Figure 3: C-type grid used in simulations

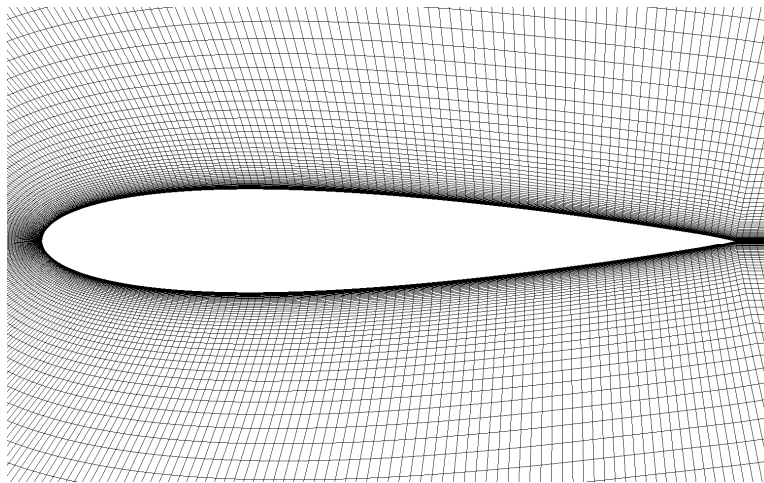


Figure 4: detailed view of grid near airfoil surface

Non-actuated airfoil performance and characteristics

In order to see whether plasma actuation has any effect on airfoil performance at all, it is necessary to compare the actuated airfoil to a non-actuated airfoil. In this section, performance and characteristics of the unactuated airfoil will be evaluated. Using the grid as defined in the previous section and by varying only the angle of attack, data was gathered from which below plots were extracted.

The flow conditions used to model this case are largely taken in a way such that it can be compared to previous work from within the laboratory. The freestream Mach number is set to 0.2. This allows for assumption of incompressible flow. The Reynolds number, as discussed in the assignment introduction and approach, is set to 1000, based on chord length. Physical chord length is 0.10m, but for use of the CFD code, the chord length has been non-dimensionalized to always be 1. Specific heat ratio and Prandtl number have been set as 1.4 and 0.72 respectively.

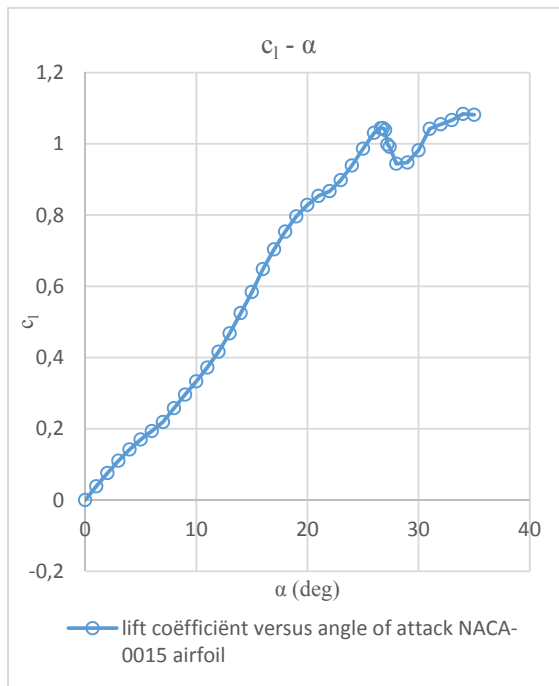


Figure 5: lift coefficient vs. angle of attack

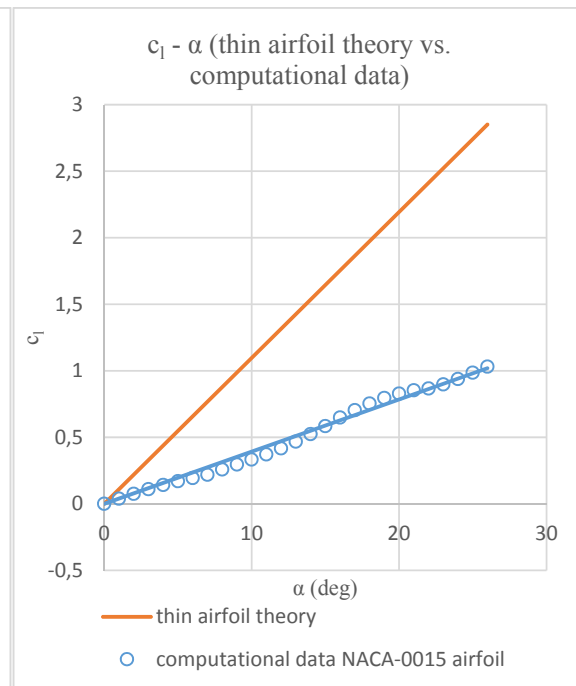


Figure 6: $c_l - \alpha$ curves, thin airfoil theory vs. computational data

From Figure 5 it can be seen that the curve showing lift coefficient versus angle of attack behaves in a familiar fashion. Stall occurs at around 26 degrees and in the pre-stall region the lift coefficient increases (nonlinearly) with increasing angle of attack. Also, since the NACA-0015 airfoil is symmetrical, the curve passes through the origin, having zero lift at angle of attack zero degrees. In figure 6, a comparison between classical two-dimensional thin airfoil theory and the computational data as found from the unactuated simulations, is made. Since

classical thin airfoil theory only predicts the linear pre-stall region, only these regions have been compared, omitting stall and post-stall data. Two apparent distinctions between the classical thin airfoil theory and the computational data can be made. Firstly, the computational data does not exactly follow a straight line (as has been drawn for illustrative purposes only, based on a least squares linear fit). This can be explained by the fact that the flow in classical thin airfoil theory is assumed to be a potential and fully attached flow. From computational data and flow field visualizations it became clear that, even for angles of attack far from stall, flow does separate in the unactuated case. Depending on how the flow behaves after separation, the pre-stall part of the lift curve behaves nonlinear. Secondly, the slope of the lift curve from computational data does not come close to the slope achieved by classical thin airfoil theory (2π). Again, the explanation for this behavior is found in the assumption that the flow is potential and fully attached in classical thin airfoil theory and that the actual flow from computations is separated. This separated flow causes a drop in lift coefficient and thus a lift curve with a slope less than that of classical thin airfoil theory.

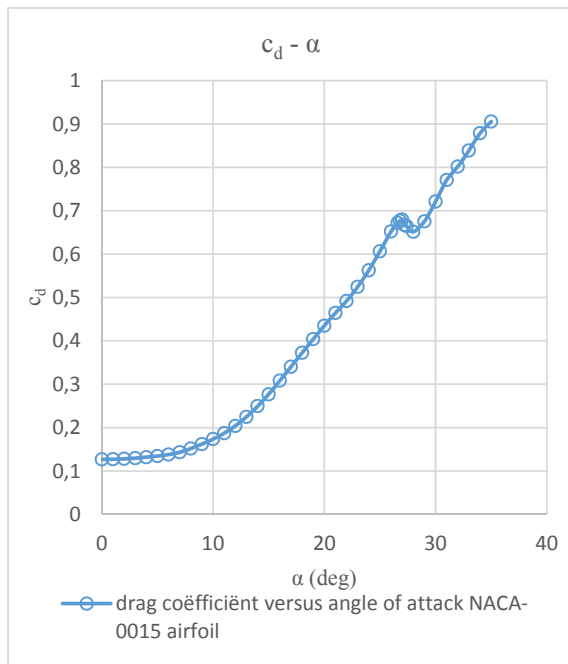


Figure 7: drag coefficient vs. angle of attack

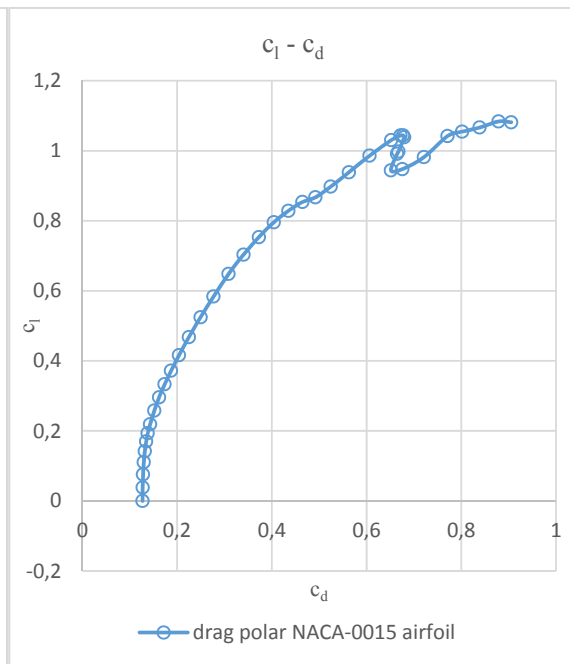


Figure 8: drag polar

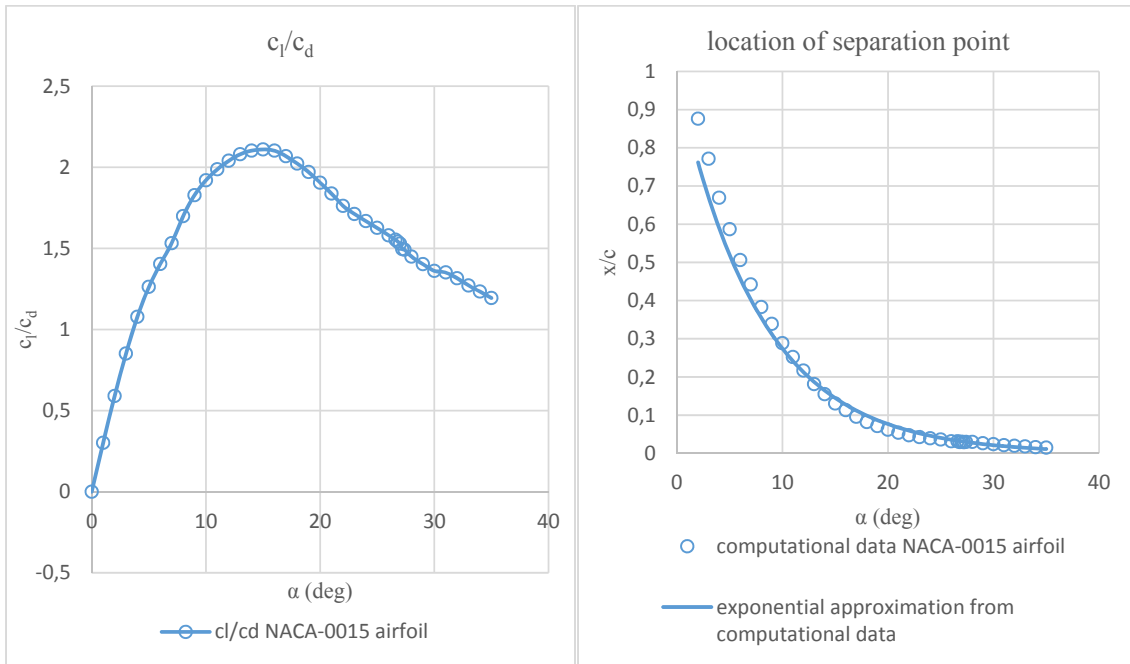


Figure 9: lift over drag vs. angle of attack, airfoil performance Figure 10: location of separation point vs. angle of attack

Figures 7 to 10 do not need much discussion as they appear to be as expected. From figure 10 it can be noted that, with increasing angle of attack, the point of separation moves from trailing edge towards leading edge in a seemingly exponential fashion.

In summary, the above curves and characteristics will be used as a reference with which the actuated airfoil data will be compared. Predictions which underlie this study are that lift might be increased, drag might be decreased, overall airfoil performance might be increased and stall and separation point might be delayed.

Determination of double zoned grid

As stated already in the assignment introduction and approach, the presence of the plasma actuator is modeled in the CFD code as an added body force. A little more precisely stated, at ISAS a general force representation has been made which is customized for every simulation. This force representation contains local information of the plasma actuator effect and is added to the existing C-type structured grid. In contrast to the reference airfoil characteristics, which were determined from simulations on a single zoned grid, the actuated airfoil characteristics are determined from this complemented, double zoned grid.

At the basis, the original C-type structured grid will cover the majority of the grid points needed to compute the data for all actuated cases. In the vicinity of the plasma actuator, however, the grid containing the plasma actuator effect will be added. This means that for every single simulation of an airfoil with plasma actuator a new grid has to be made. Referring to chapters to come for the more elaborate explanation, this means that 19 different grids have been created, apart from the original C-type grid.

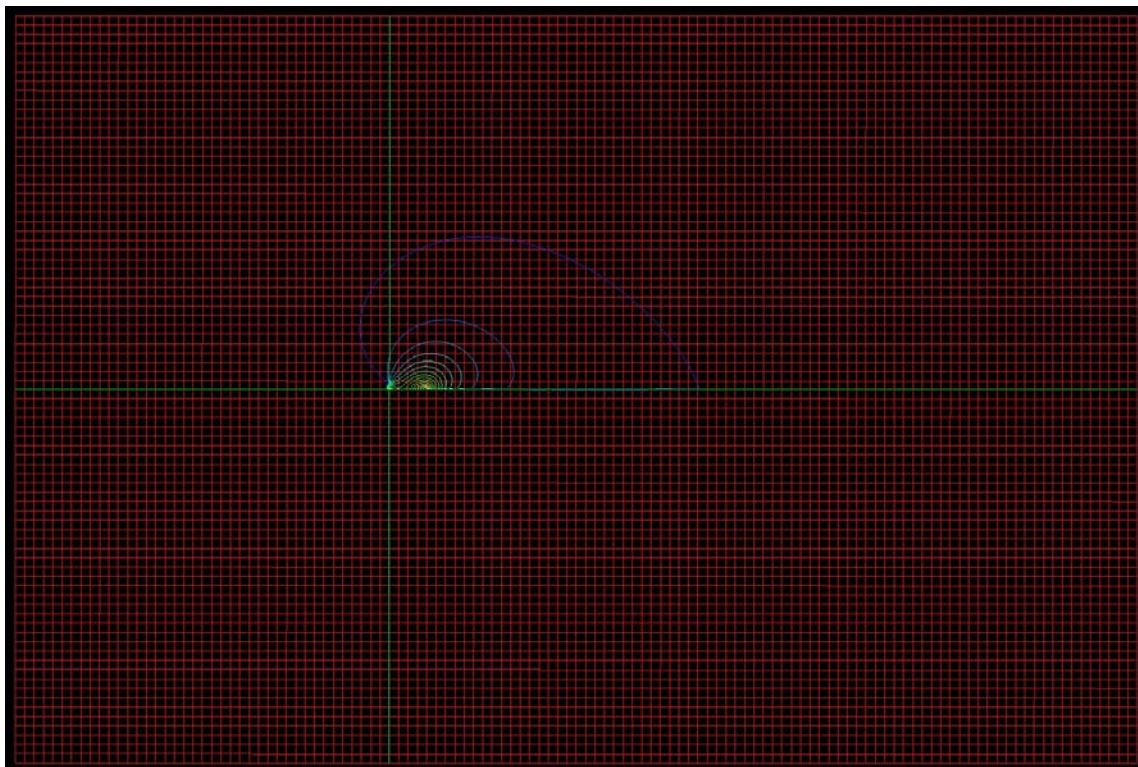
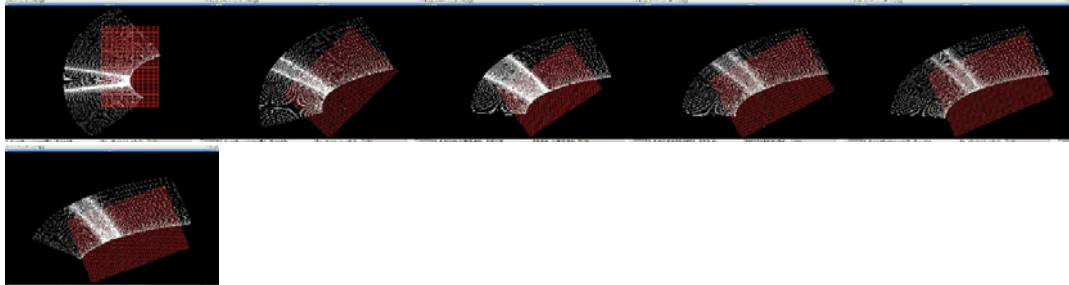


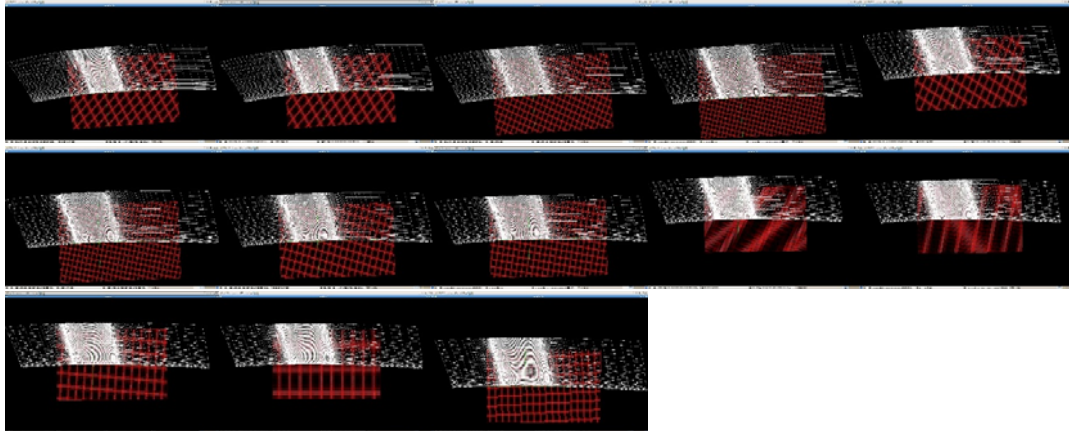
Figure 11: plasma actuator body force representation

In figure 11 it is shown how the body force is modeled. The intersection of the green lines represent the point where the plasma actuator is located. This point should be matched with the location on the airfoil surface where the actuator is present. The colored lines originating from this intersection represent the body force added to the conservation equations.

Because the grid containing the body force information is so much finer than the original C-type grid, an intermediate grid is needed to transfer the information from the body force database onto the C-type grid. In the figures below, the body force mapping can be seen as the red square and the intermediate grid can be seen as the white grid, partially covering the airfoil surface. Again, a more detailed description as to what pre- and post-stall regions are will follow in the chapter to come.



Figures: Post-stall region actuator location grids



Figures: Pre-stall region actuator location grids

Actuated airfoil performance and characteristics

In this chapter, the plasma actuator will be added to the airfoil. It should be noted that all curves and characteristics are obtained under normal actuation, unless clearly stated otherwise. In this case, normal actuation refers to continuous actuation. Also, flow conditions are set to be equal to those of the reference case. The only exception to this are of course the settings of the actuator. The CFD code accepts two settings related to the plasma actuator, actuation mode and the non-dimensional plasma scale parameter, D_c . The value for actuation mode is set to 1 (representing 100%, or normal, actuation) and the value for D_c is set to 0.5. This value is based on best practices from within JAXA.

In this study, several different applications of the plasma actuator are looked into. Not just a noticeable effect of the actuator is of importance, but also, if possible, some understanding and optimization of effects would be desirable. Therefore, several aspects are taken into account. The most important of these aspects is optimal actuator location. Second important aspect is the mode of actuation and how this affects the effect the actuator has on airfoil performance.

It would be interesting to look at many actuator locations and operating modes at all the angles of attack from which the reference lift curve is created. This would be enormously time-consuming, however. It is therefore chosen only to look at two regions on the lift-curve. First region is the pre-stall region, somewhere halfway towards stall, at angles of attack 10, 11 and 12 degrees. The second region is the post-stall region at angles of attack 27, 28 and 29 degrees. For those six angles of attack the plasma actuator is added at different locations on the airfoil surface. Also, for two of those angles of attack, 11 and 28, the operation mode is changed for a fixed actuator location. Although it doesn't cover all the possibilities for actuator optimization, it should give some idea about the workings.

From previous studies into plasma actuation, it is known that actuating near separation point is most effective, whereas actuating far from the separation point has close to no influence on airfoil performance at all. In the pre-stall region, it can be seen from figure 9 that separation occurs at 29%, 25% and 21% for angles of attack 10, 11 and 12 respectively. It is therefore chosen to vary actuator location between 19% and 31% of chord length from leading edge, every 1%. In the post-stall region, it can be seen from figure 9 that separation occurs at 3% for all three angles of attack, which are grouped much closer than separation points in pre-stall region. The actuator location for post-stall region is therefore chosen to vary from 0% to 5% of chord length from leading edge, every 1%. Referring to the figures at the end of the previous chapter with regard to the double zoned grids which have been used for all simulations. Each grid can be used for every angle of attack, each actuator location, however, requires a grid which has been set up for that particular actuator location. In summary, figure 12 shows what regions have been selected for actuation.

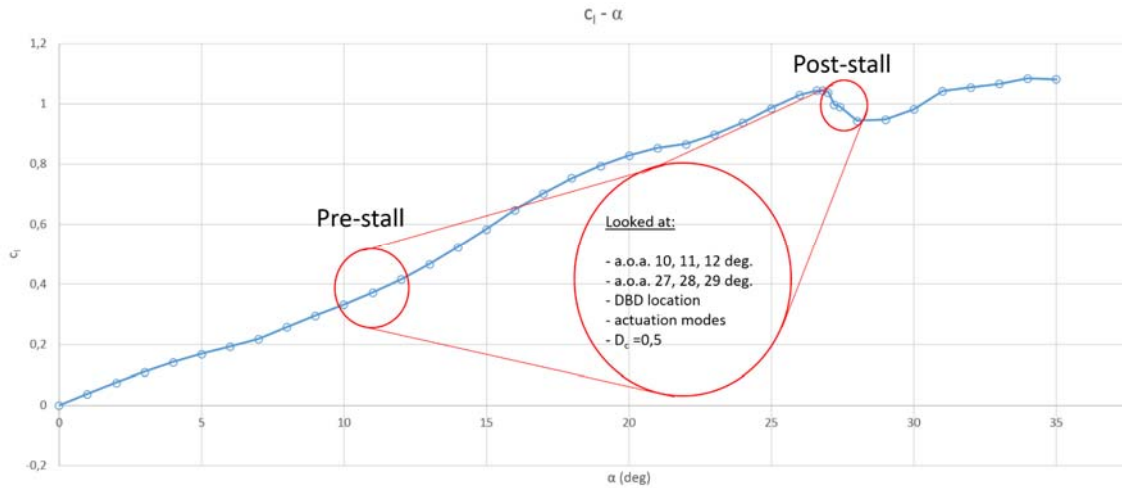


Figure 12: actuation summary

Pre-stall results

All figures below contain results from actuation at pre-stall angles of attack.

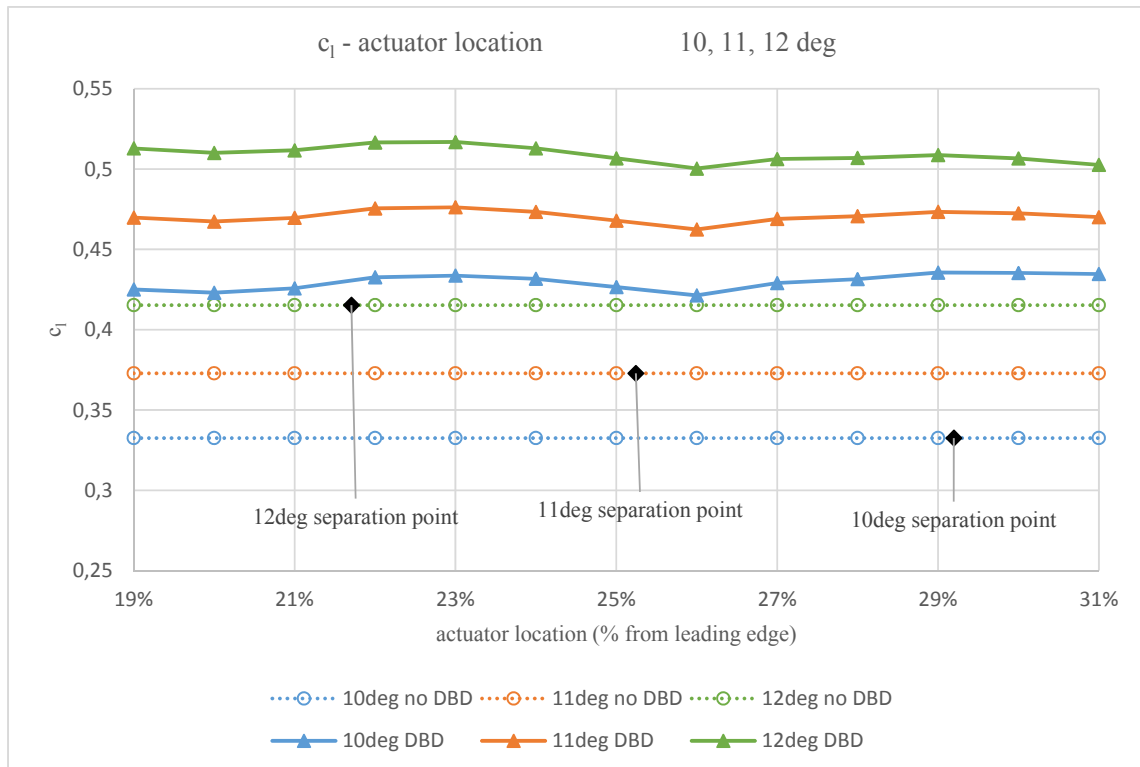


Figure 13: c_1 - actuator location, pre-stall

Figure 13 shows the results on c_1 for pre-stall, normal mode actuation with D_c 0.5 and actuator location varying between 19% and 31% chord length from leading edge. In black, the separation

points of the flow in the reference cases have been shown. A few remarks about these results can be made. What is very apparent, is that at all angles of attack, c_d definitely increases, for all actuator locations. What can also be seen is that, apart from some very small fluctuations, the increase in c_d seems to be constant and thus independent of actuator location. Keep in mind that this seems true only for the range of 19% - 31% since no simulations have been performed outside that scope. What can be concluded is that normal actuation in pre-stall region has a positive effect on lift, seemingly independent of actuator location.

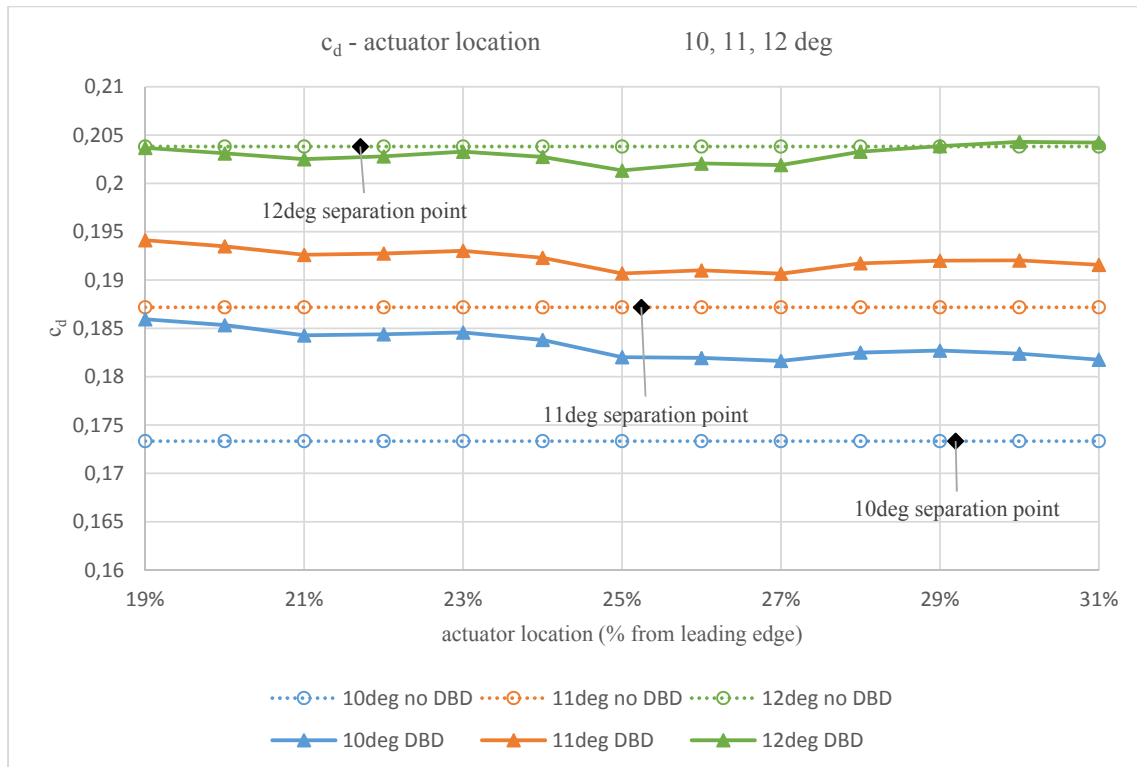


Figure 14: c_d - actuator location, pre-stall

Figure 14 shows the results on c_d for pre-stall, normal mode actuation with D_c 0.5 and actuator location varying between 19% and 31% chord length from leading edge. In black, the separation points of the flow in the reference cases have been shown. From this figure it can be seen that drag increases for angles of attack 10 and 11 degrees. If the slight variation in drag over actuator location is neglected, the increase in drag is larger for 10 degrees angle of attack than for 11 eleven degrees angle of attack. For angle of attack 12 degrees, however, drag seems to be unchanged under the influence of actuation for all actuator locations. From this plot it is impossible to be conclusive about the behavior of the drag under influence of actuation. It seems that for some angles of attack drag is increased under actuation and that there might exist a point at which drag actually is starting to decrease under the influence of actuation. More elaborate research is necessary to be conclusive.

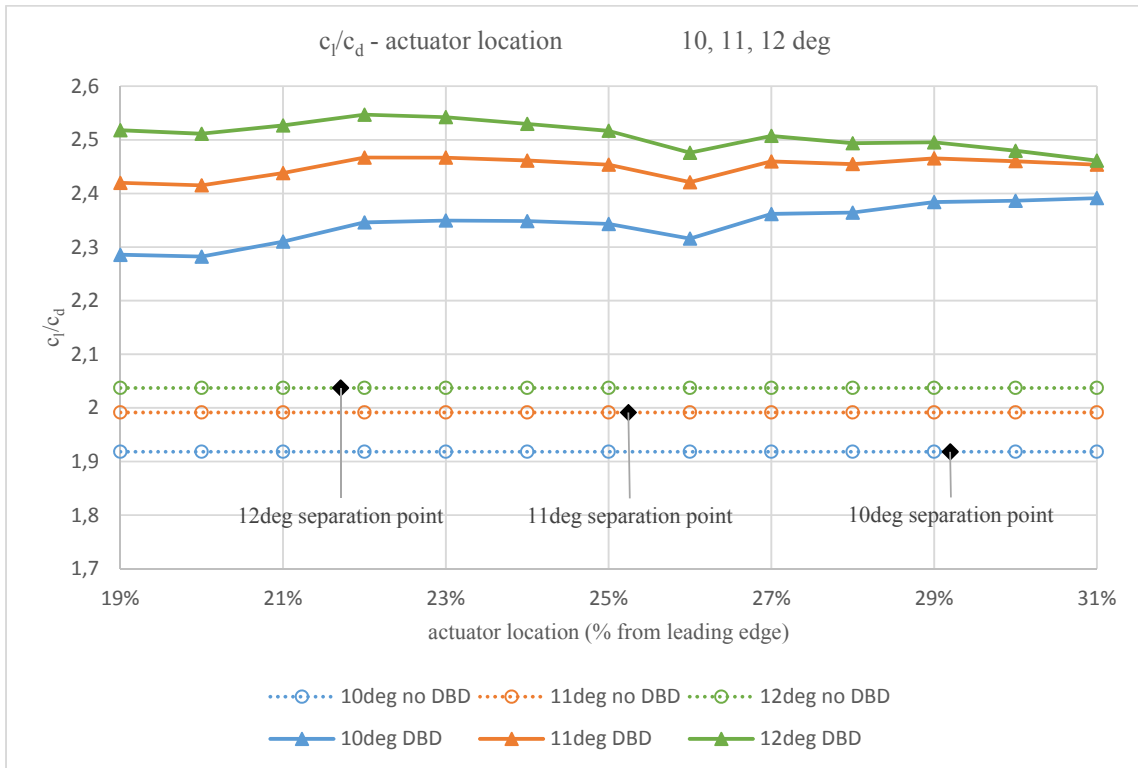


Figure 15: c_l/c_d – actuator location, pre-stall

Figure 15 shows the results on airfoil performance in terms of c_l/c_d for pre-stall, normal mode actuation with $D_c 0.5$ and actuator location varying between 19% and 31% chord length from leading edge. In black, the separation points of the flow in the reference cases have been shown. Even though it has been concluded from figure 14 that no conclusion about the behavior of the drag could be given, it is clear from figure 15 that airfoil performance increases under the influence of actuation. Considering that both lift and drag were seen to behave independent of actuator location, this is also true for its division, lift over drag. The curves might not be perfect straight lines, they should be regarded as such.

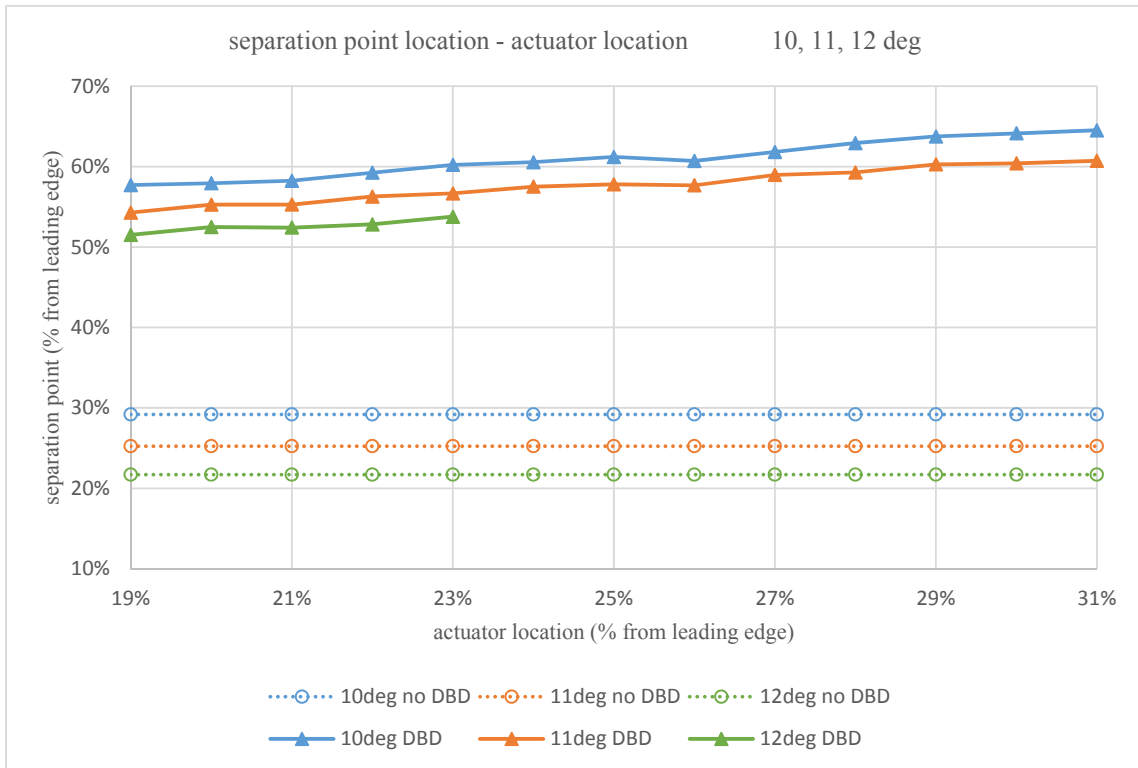


Figure 16: separation point location– actuator location, pre-stall

Figure 16 shows the results on separation point location for pre-stall, normal mode actuation with $D_c = 0.5$ and actuator location varying between 19% and 31% chord length from leading edge. Before going into the details of the results, it should be noted that data for the 12 degrees angle of attack is missing from between 23% and 31%. Since the simulations containing that information failed and there was no time left to redo them, they remain blank. Even though, the trend of the available data seems to be in agreement with the behavior of the other two cases (10 and 11 degrees) so it might be assumed that the missing data would follow this trend as well. The results show that actuation has a strong effect on separation point location, moving it further downstream towards trailing edge. It can also be seen that with actuator location moving towards trailing edge, the separation point moves even further towards trailing as well, showing some kind of dependence.

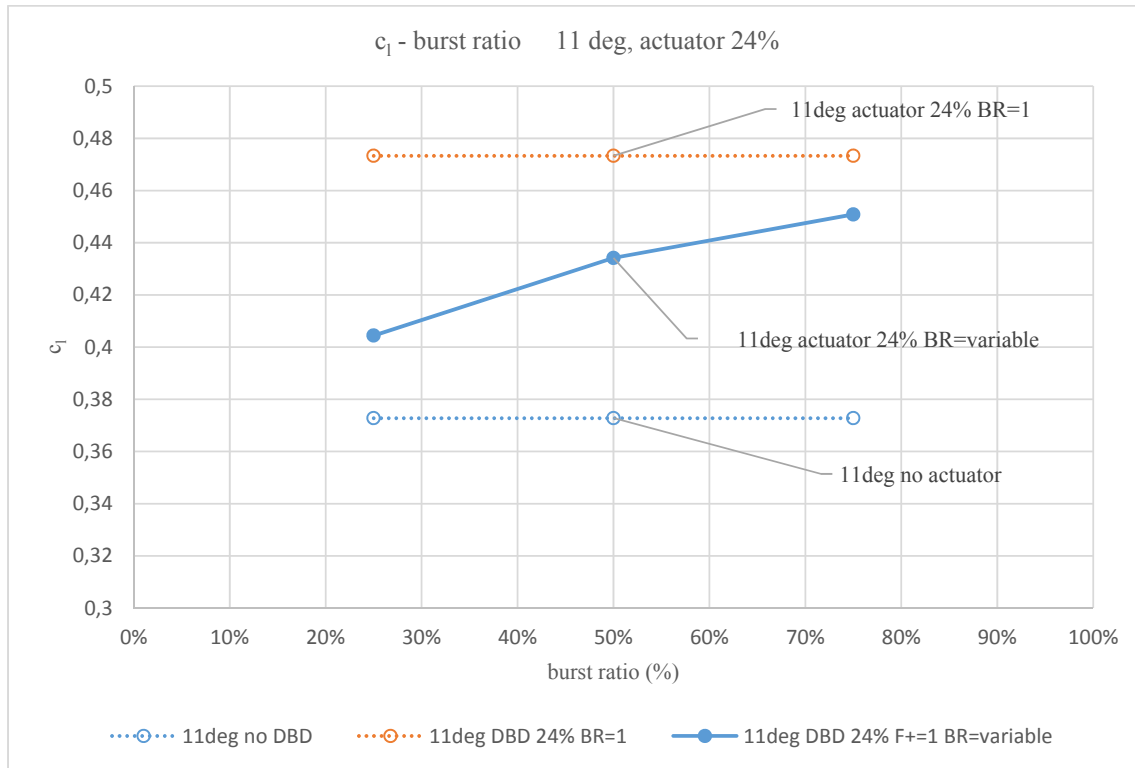


Figure 17: c_1 – burst ratio, pre-stall

Figure 17 shows results for actuation under a different actuation mode, burst mode. In this case, the actuation has been switched off for certain periods of time. The timescale used is the convective time, or, the time it takes for a flow element to have travelled an entire chord's length. Based on that time, we have already seen the results for 100% on, or normal mode actuation. In this plot, effects on lift have been shown for 25%, 50% and 75% burst ratio, or, percentage of convective time of which is actuation is turned on. Also, this plot shows only results for one particular angle of attack and one particular actuator location. What can clearly be seen is that actuation in burst mode increases lift compared to unactuated case but never reaches the level of increase as normal mode actuation does. It can be seen that, as burst ratio approaches 100% or normal mode, lift approaches the level of normal mode actuation. Though this plot only shows results on lift, the data on drag, lift over drag and separation point location are available and show similar behavior. Those plots have not been shown. It can be concluded that actuation in burst mode is less effective than operation in normal mode, based on a convective timescale.

It has been suggested to change the timescale from convective time to the timescale with which vortices are shedded (Strouhal vortex shedding frequency). Actuating at vortex shedding frequency has proved in previous works to effectively change the direction of the separated shear layer towards the airfoil surface (the second mechanism of the plasma actuator effect) and be more effective than normal actuation. Because of time restrictions these simulations have not been conducted.

Post-stall results

All figures below contain results from actuation at post-stall angles of attack.

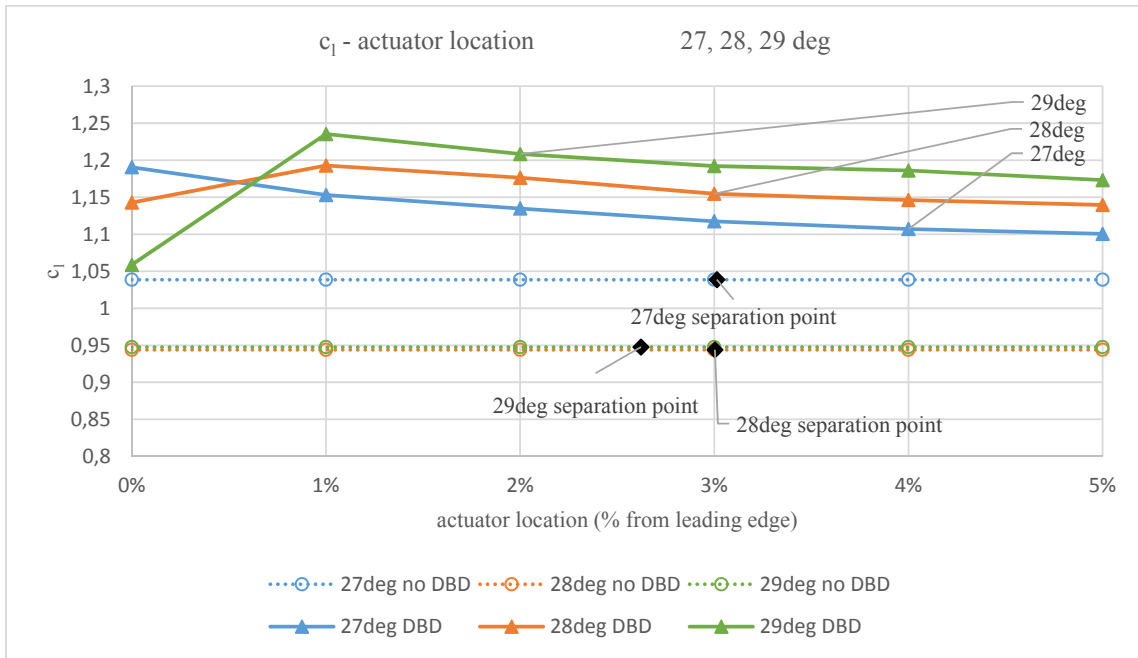


Figure 18: c_l – actuator location, post-stall

Figure 18 shows the results on lift for post-stall, normal mode actuation with $D_c 0.5$ and actuator location varying between 0% and 5% chord length from leading edge. In black, the separation points of the flow in the reference cases have been shown. What can be observed is that for all simulated actuator locations lift increases. Also, there seems to be a maximum increase in lift for actuation at around 1% or 2% of chord's length. The further the actuator is moved downstream, the less effective it seems to become.

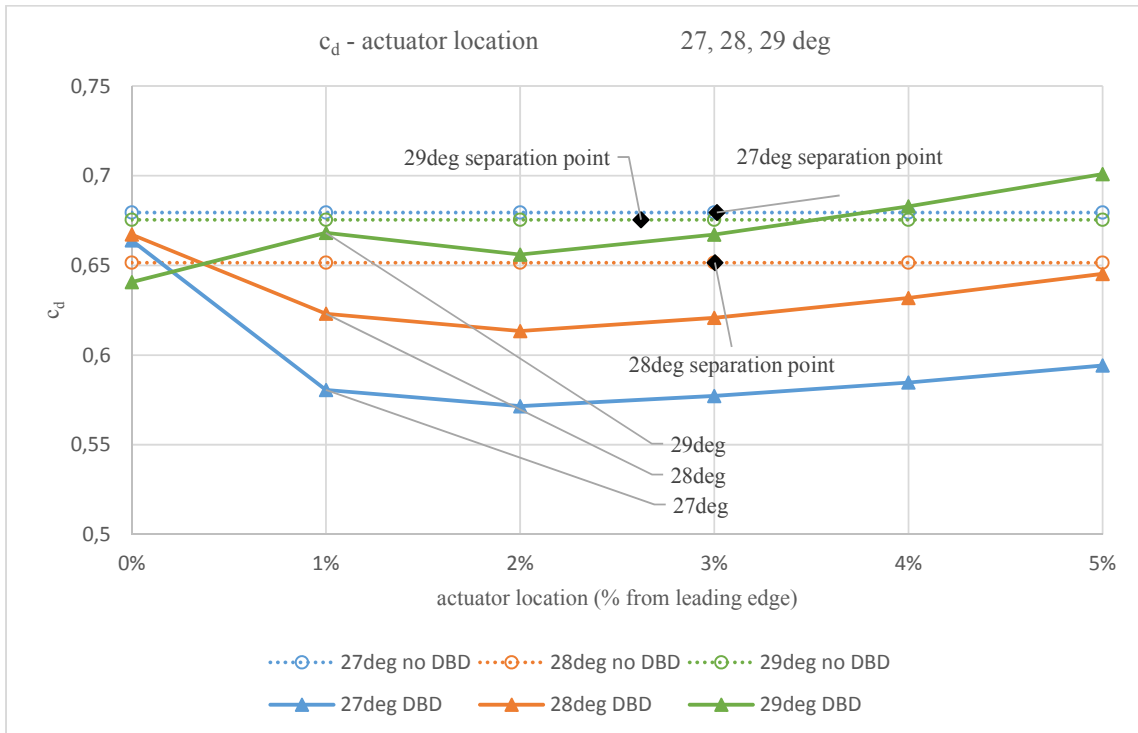


Figure 19: c_d – actuator location, post-stall

Figure 19 shows the results on drag for post-stall, normal mode actuation with D_c 0.5 and actuator location varying between 0% and 5% chord length from leading edge. In black, the separation points of the flow in the reference cases have been shown. From the figure it can be seen that there are actuator locations for which the drag decreases and that there are locations for which the drag increases. In general, there seems to be an optimum actuator location at around 2% of chord's length. With the actuator location behind unactuated separation points, drag decrease diminishes quickly and might even turn into drag increase.

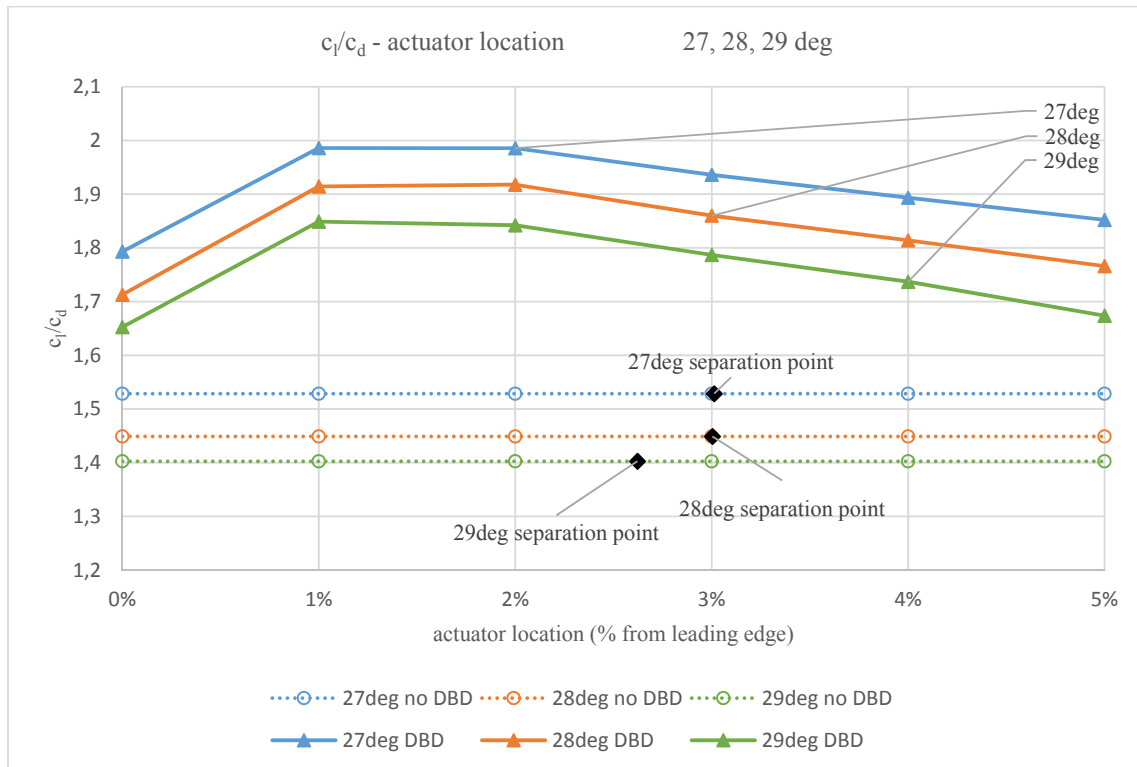


Figure 20: c_l/c_d - actuator location, post-stall

Figure 20 shows the results on airfoil performance in terms of c_l/c_d for post-stall, normal mode actuation with D_c 0.5 and actuator location varying between 0% and 5% chord length from leading edge. In black, the separation points of the flow in the reference cases have been shown. It is clearly visible that actuation at all actuator locations increase the airfoil performance. At around 2% of chord's length, actuating has an optimum.

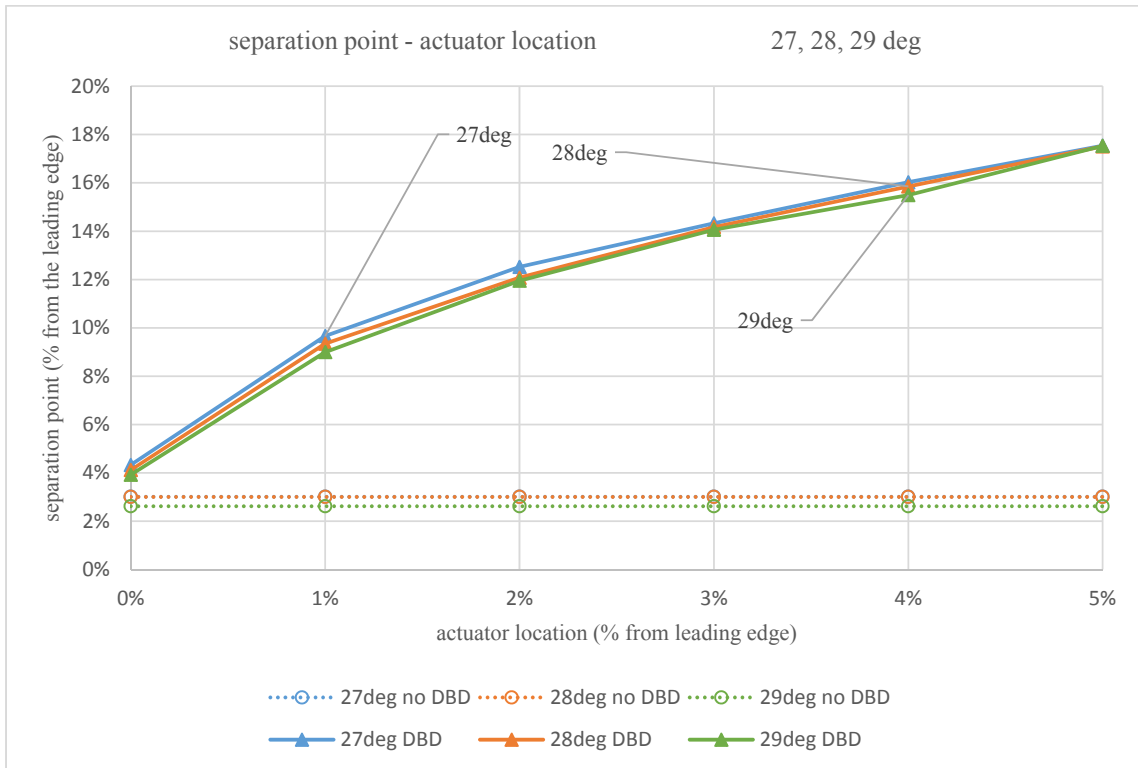


Figure 21: separation point location – actuator location, post-stall

Figure 21 shows the results on separation point location for post-stall, normal mode actuation with $D_c 0.5$ and actuator location varying between 0% and 6% chord length from leading edge. It is observed that separation point is moved further downstream for any actuator location. As is the case for pre-stall angles of attack, for post-stall angles of attack the separation point moves further downstream with increasing actuator location, in a nonlinear fashion. Separation point location is dependent of actuator location in post-stall region.

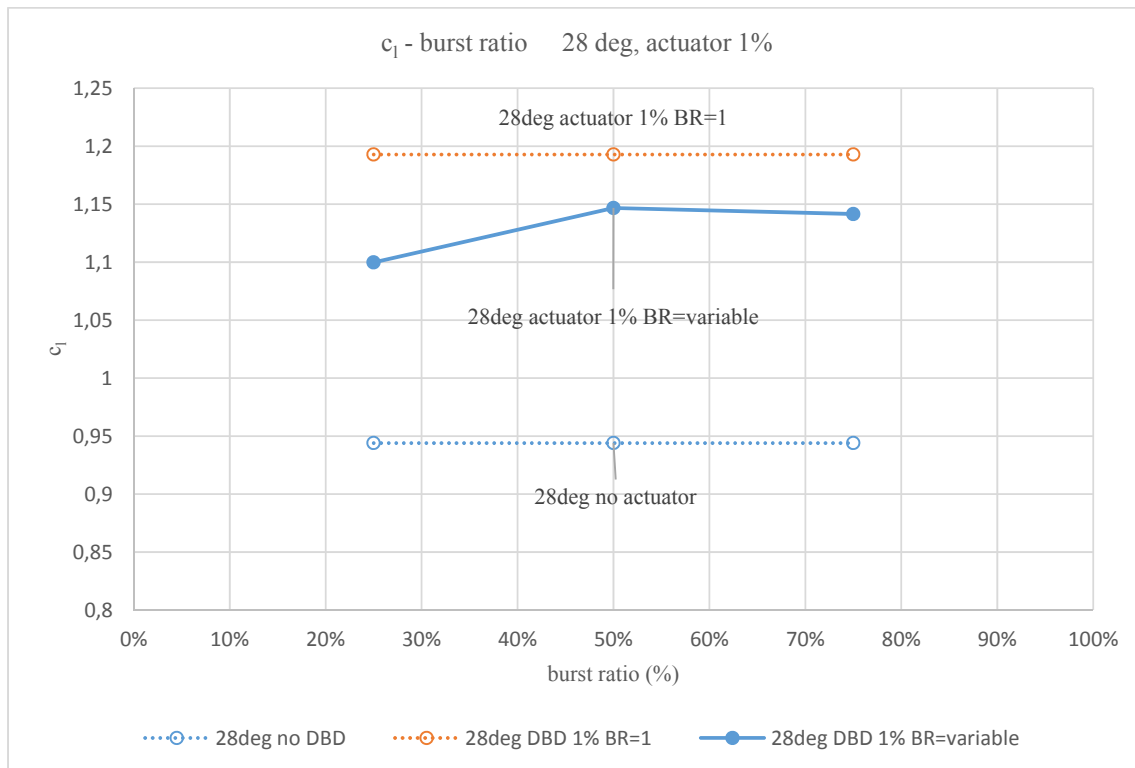


Figure 22: c_1 - burst ratio, post-stall

For post-stall angles of attack, similar simulations have been performed regarding the second actuation mode, burst actuation. As could be seen at pre-stall angles of attack in figure 17, lift is increased compared with unactuated case, but not increased as much as for normal mode actuation. This behavior is also seen in the data on lift, drag, lift over drag and separation point for post-stall region. The same suggestion concerning the timescale for the burst mode actuation is valid for the post-stall angles of attack.

In summary it is seen that for pre-stall angles of attack, lift is increased independent of actuator location, within the region of 19% to 31% actuator location. Drag is also increased independent of actuation location though at 12 degrees angle of attack there does not seem to be any influence on drag at all from the actuator. To be conclusive about drag in pre-stall angles of attack more elaborate simulations need to be conducted. Airfoil performance is increased for pre-stall angles of attack independent of actuator location and separation point moves further downstream as the actuator moves further downstream, showing dependency on actuator location. Burst mode actuation based on a convective timescale is more effective than no actuation at all, but less effective than normal mode actuation.

For post-stall angles of attack, lift is increased with an optimum actuator location at around 1% of chord length. Drag is decreased with an optimum actuator location at around 2% of chord length. Airfoil performance has an optimum increase at actuator location 2% of chord length and separation point moves further downstream with increasing actuator location. Burst mode actuation based on a convective timescale is more effective than no actuation at all, but less effective than normal mode actuation.

Comparison non-actuated and actuated cases

This chapter summarizes all data so far and looks into general statements regarding the influence and effectiveness of the plasma actuator.

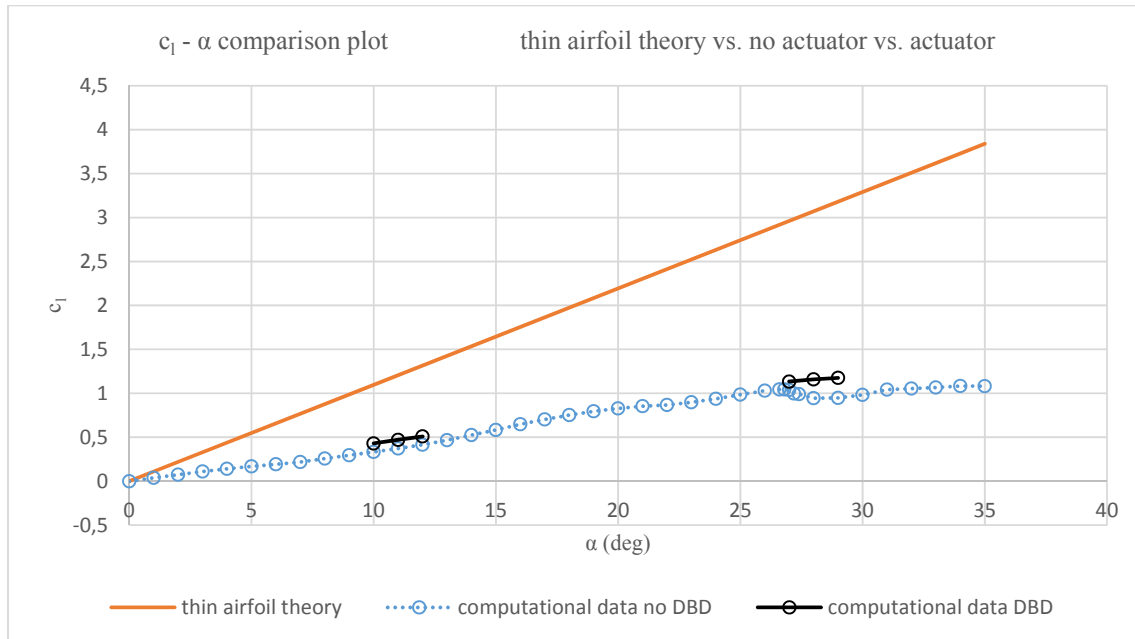


Figure 23: $c_l - \alpha$ comparison plots

Figure 23 shows the original, unactuated lift curve, the classical thin airfoil prediction of the lift curve and the values of lift coefficient for pre- and post-stall regions under the influence of plasma actuator. The values of lift coefficient taken for the actuated regions are the averaged values of the lift coefficient over actuator location for the pre-stall region (since the increase in lift coefficient is independent of location) and the values at actuator location 2% of chord length for the post-stall region (since airfoil performance was optimal for actuating at 2% of chord length). Is it realistic to show a single graph with data of multiple actuator locations? For research purposes it simply shows what is possible, for practical purposes this would mean that the airfoil should be equipped with at least two plasma actuators (maybe even more if the entire data set becomes available). More than one actuator on an airfoil is quite unusual though it can be imagined that a parallel series of actuators is installed on the airfoil.

From this figure two main statements can be made. Firstly, for pre- and post-stall regions, the lift curve is increased towards the theoretical thin airfoil lift curve. Secondly, for post-stall region, the lift curve is lifted from deep stall to what seems to be a continuation of the pre-stall region. This means stall is delayed. Since the simulations are limited to six angles of attack only, no information on the new, delayed, stall angle exists. Both phenomena are desirable as they makes the airfoil perform better and more efficient.

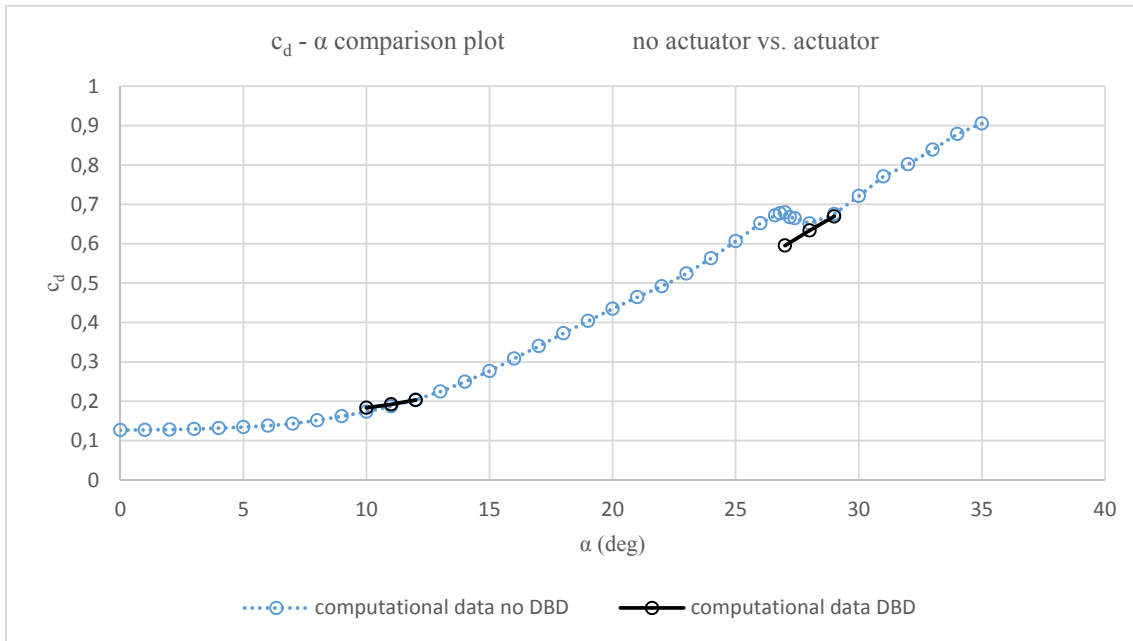


Figure 24: $c_d - \alpha$ comparison plots

From figure 24 it can be seen that for pre-stall angles of attack drag is not that much affected by the actuator's presence. It must be stated, however, that no conclusive statement could be made in the previous chapter on actuator location and the influence on drag. What this figure might suggest is that at around 11 or 12 degrees angle of attack drag could change from being increased (at very low angles of attack) to being decreased (at higher than 11 or 12 degrees), compared to the unactuated case. Purely speculative though, this needs to be investigated further by means of more simulations at different angles of attack. Next to this, it can be seen that drag for the post-stall region is decreased, though it catches up quickly with the original curve. This plot does not reveal that much apart from the fact that drag just after stall is significantly decreased. As stated in the previous chapter, more simulations need to be conducted in order to make conclusive statements.

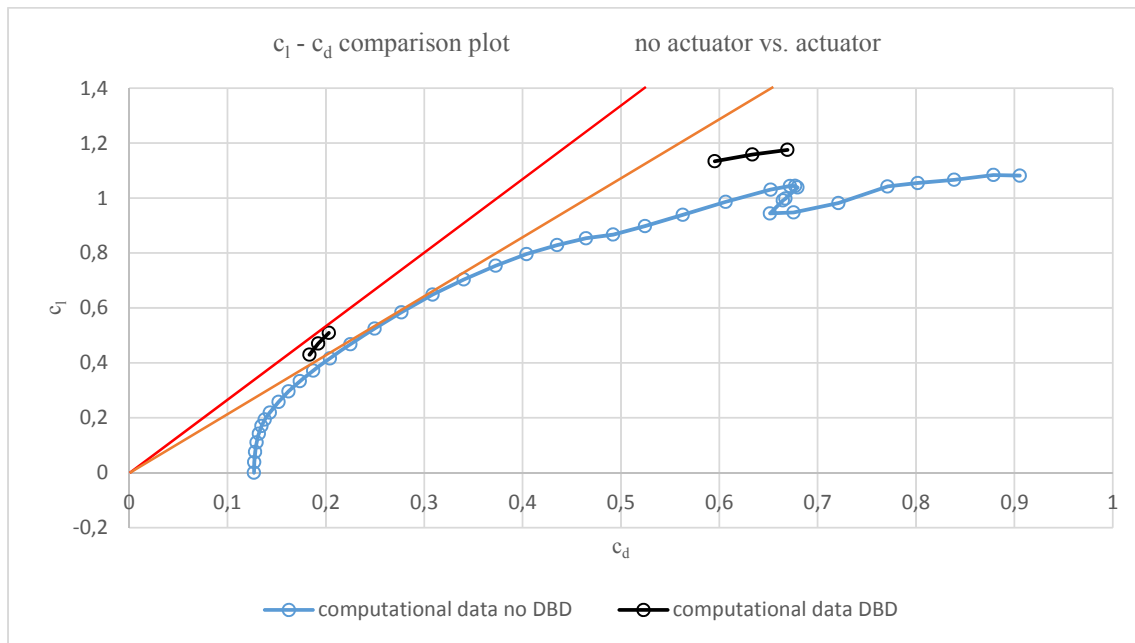


Figure 25: drag polar comparison plots

The above figure shows an important image. Both pre- and post-stall regions show an improvement in c_l compared to c_d . This means that at equal lift, drag is reduced, or, at equal drag, the lift is increased. What this picture also shows are (albeit approximate) the lines defining the point of highest lift over drag. For the unactuated case this is represented by the orange line whereas this is shown for the actuated case by the red line. The tangent from the origin to the drag polar defines this point. As can be seen is that (even for the data in the limited pre- and post-stall regions) the slope of the tangent for the actuated case is greater than the slope of the tangent of the unactuated case. This could have severe implications for practical flight dynamics. For instance, cruising speed of aircrafts (for similar airfoil and flow conditions) could be increased, reducing flight time. Drag could also be reduced for aircrafts in stationary flight, reducing fuel consumption and saving costs.

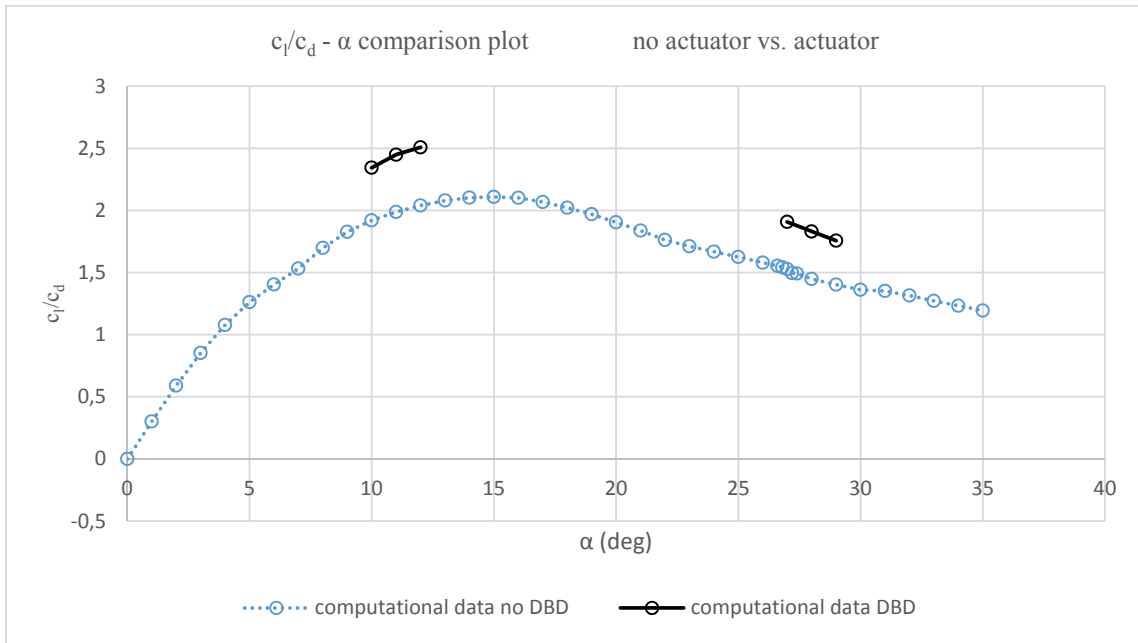


Figure 26: $c_l/c_d - \alpha$ comparison plots

Figure 26 shows airfoil performance in terms of c_l/c_d for both the unactuated and the actuated cases. It can clearly be stated that airfoil performance for both the pre- and post-stall regions is increased. From this, the same conclusions can be drawn as have been at the previous section regarding the drag polar, which will not be repeated here. Though speculative, because no data on actuation between 12 and 27 degrees angle of attack exists, it could be reasoned that the point of highest c_l/c_d is moved from about 15 degrees angle of attack in unactuated case to around 16 or 17 degrees angle of attack in actuated case.

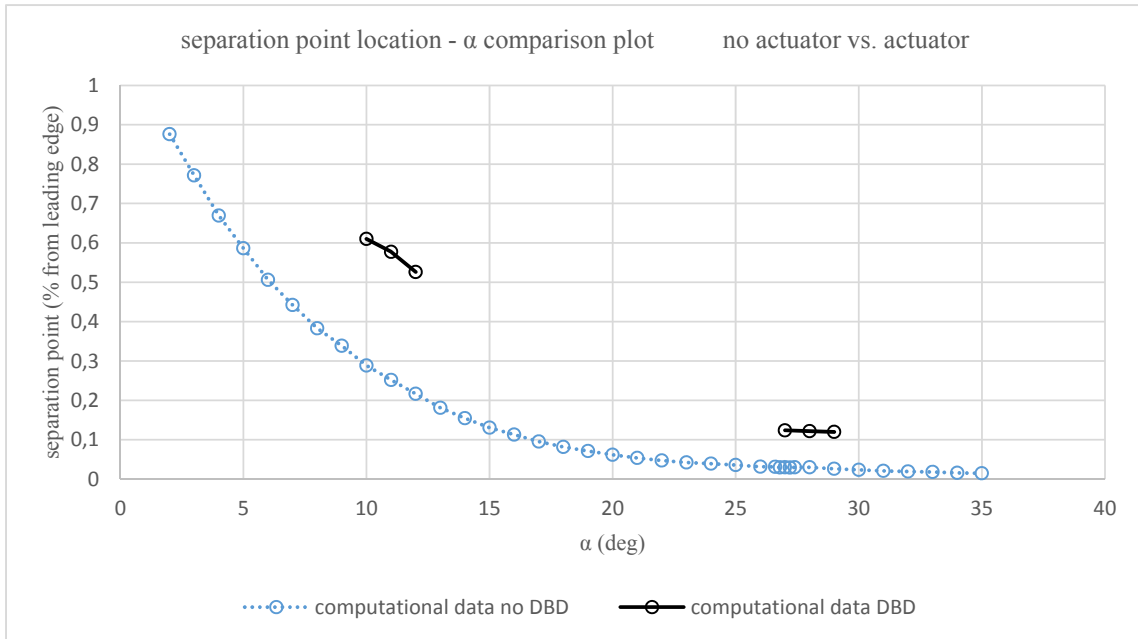
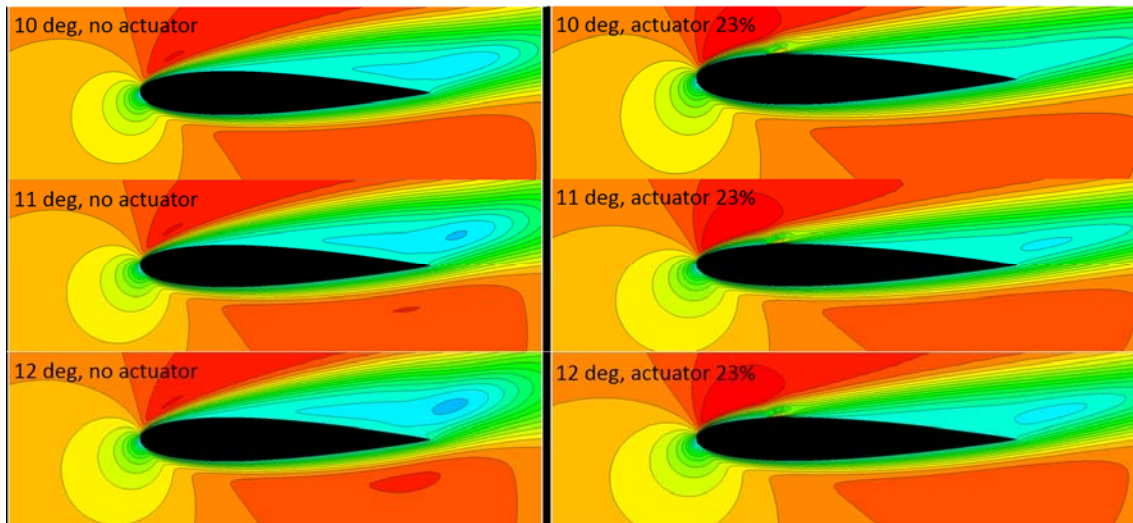
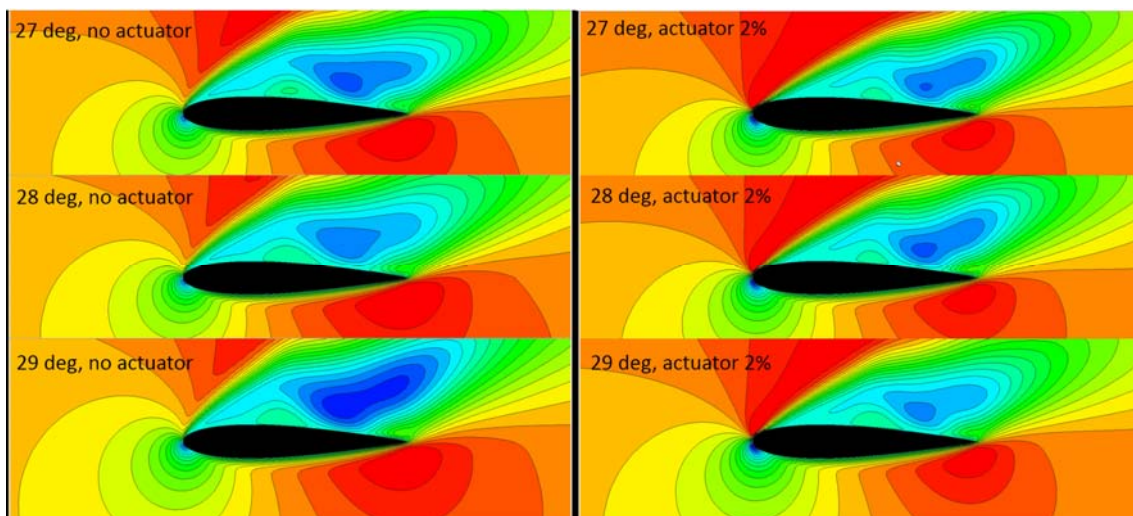


Figure 27: separation point location - α comparison plots

Simply stated, from figure 27 it becomes clear that the separation point, under the influence of actuation, moves further downstream. It should be interpreted as the curve being shifted upwards. Separation is delayed and the flow stays more attached to the airfoil. To give a visual presentation of what this means, the figures below show averaged flow fields for pre- and post-stall regions in unactuated and actuated cases. The images show horizontal flow velocity gradients and have been time averaged. The images clearly show the actuator presence and the effect on separation point. For pre-stall regions, the actuator is at 23% of chord length since that was the final actuator location for which data on separation point was available (see previous chapter). For post-stall region, the actuator has been placed at 2% of chord length since increase in airfoil performance was optimal for actuating on this location.



Figures: pre-stall time-averaged flow field plots, horizontal flow velocity, unactuated vs. actuated (at 23%)



Figures: post-stall time-averaged flow field plots, horizontal flow velocity, unactuated vs. actuated (at 2%)

Conclusion and recommendations

From all the analysis, some conclusions can be drawn. First of all, unactuated airfoil performance is much worse than predicted by classical thin airfoil theory, because of pre-stall flow separation from the actual airfoil. It was shown that for pre-stall angles of attack, lift and lift over drag are increased and separation is delayed under influence of normal actuation, independent of actuator location. Because of inconclusive data, no general statement about the behavior of drag under the influence of normal actuation could be made. For post-stall angles of attack, lift is seen to increase with a clear optimum under the influence of normal actuation, as is airfoil performance. Drag is seen to decrease with a clear optimum under the influence of normal actuation and separation is seen to be delayed, dependent on actuator location. For both pre- and post-stall regions, burst mode actuation based on convective timescale is less effective as normal actuation.

In general, the actuated airfoil performs better than the unactuated airfoil, seeing an increase in the slope of the lift curve towards the classical thin airfoil theory curve. Also, stall is delayed and aircraft cruising conditions could be improved to higher cruising speeds or more economical flight conditions.

Some recommendations are necessary for completeness. First of all, more pre-stall simulations at different angles of attack are necessary to be conclusive about drag behavior under the influence of normal actuation. As a matter of fact, to have a more complete insight in what happens over the entire range of angles of attack, many more (preferably all) angles of attack need to be simulated under the influence of actuation. Also, a wider range of actuator locations should be considered. Burst mode actuation proved to be less effective than normal mode actuation if based on the convective timescale. Burst mode actuation based on different timescales, such as the vortex shedding timescale, should be simulated for a wide range of situations. Lastly, it would be interesting to have some experimental validation. Though it is quite difficult to meet flow conditions in real wind tunnels and current plasma actuators might not be as precise as simulated, any data is welcome.

References

Ramakumar, K., and Jacob, J. D., "Flow Control and Lift Enhancement Using Plasma Actuators," *AIAA-2005*, 2005

Post, M. L., and Corke, T. C., "Flow Control with Single Dielectric Barrier Plasma Actuators," *AIAA 2005-4630*, 2005

Vey, S., Nayeri, C.N., and Paschereit, C.O., "Plasma Flow Control on Low Aspect Ratio Wings at Low Reynolds Numbers," *AIAA 2010-1222*, 2010

Suzen, Y. B., and Huang, P. G., "Simulations of Flow Separation Control using Plasma Actuators," *AIAA 2006-877*, 2006

Corke, T. C., Jumper, E. J., Post, M. L., and Orlov, D., "Application of Weakly-Ionized Plasmas as Wing Flow-Control," *AIAA 2002-0350*, 2002

Post, M. L., and Corke, T. C., "Separation Control on High Angle of Attack Airfoil Using Plasma Actuators," *AIAA 2003-1024*, 2003

Cho, Y. C., "Low-Reynolds Number Adaptive Flow Control Using Dielectric Barrier Discharge Actuator," *Book*, 2010

Greenblatt, D., Göksel, B., and Rechenberg, I., "Dielectric Barrier Discharge Flow Control at Very Low Flight Reynolds Numbers," *AIAA 2007-1452*, 2007

Tsubakino, D., Tanaka, Y., and Fujii, K., "Effective Layout of Plasma Actuators for a Flow Separation Control on a Wing," *AIAA 2007-474*, 2007

Greenblatt, D., Schneider, T., and Schule, C. H., "Mechanism of flow separation control using plasma actuation," *Phys. Fluids 24*, 077102, 2012

Nonomura, T., Aono, H., Sato, M., Yakeno, A., Okada, K., Abe, Y., and Fujii, K., "Control Mechanism of Plasma Actuator for Separated Flow around NACA0015 at Reynolds Number 63,000 Separation Bubble Related Mechanisms," *AIAA 2013-0853*, 2013

Aono, H., Okada, K., Nonomura, T., Kawai, S., Sato, M., Yakeno, A., and Fujii, K., "Effects of Burst Frequency and Momentum Coefficient of DBD Actuator on Control of Deep-stall Flow around NACA0015 at $Re_c=2.6 \cdot 10^5$," *AIAA 2014*, 2014